Calphad 63 (2018) 142–147

Contents lists available at ScienceDirect

Calphad

journal homepage: www.elsevier.com/locate/calphad

First principles phase diagram calculation for the 2D TMD system $WS_2 - WTe_2$

B.P. Burton[a,*], M.H.F. Sluiter[b]

[a] Materials Measurement Laboratory, National Institute of Standards and Technology (NIST), Gaithersburg MD 20899, USA
[b] Department of MSE/3ME, Delft University of Technology, Mekelweg 2, 2628 CD Delft, the Netherlands

ARTICLE INFO

Keywords:
WS2 – WTe2
First principles
Phase diagram calculation
Van der Waals
Transition metal dichalcogenide
TMD

ABSTRACT

First principles phase diagram calculations, that included van der Waals interactions, were performed for the bulk transition metal dichalcogenide system $(1-X)\cdot WS_2 - (X)\cdot WTe_2$. To obtain a converged phase diagram, a series of cluster expansion calculations were performed with increasing numbers of structural energies, (N_{str}) up to $N_{str} = 435$, used to fit the cluster expansion Hamiltonian. All calculated formation energies are positive and all ground-state analyses predict that formation energies for supercells with 16 or fewer anion sites are positive; but when $150 \lessapprox N_{str} \lessapprox 376$, false ordered ground-states are predicted. With $N_{str} \geq 399$, only a miscibility gap is predicted, but one with dramatic asymmetry opposite to what one expects from size-effect considerations; i.e. the calculations predict more solubility on the small-ion S-rich side of the diagram and less on the large-ion Te-rich side. This occurs because S-rich low-energy metastable ordered configurations have lower energies than their Te-rich counterparts which suggests that elastic relaxation effects are not dominant for the shape of the miscibility gap.

1. Introduction

There is great interest in two-dimensional (2D) transition metal dichalcogenide (TMD) materials MX_2, where M = Mo, W, Nb, Re, etc. and X = S, Se, or Te. [1,2]. Currently, interest is focused on applications such as: band-gap engineering [3,4]; nano-electronic devices [2,5–7]; photovoltaic devices [8,9]; valleytronics applications [10,11]; 2D building blocks for electronic heterostructures [12]; and as sensors [13].

The bulk 2 H crystal structure ($P6_3/mmc$ space group) has AB-stacking of three-atom-thick 2D-layers that are bonded by van der Waals forces. Hence van der Waals forces influence bulk and multilayer phase relations and therefore anion order-disorder and/or phase separation in TMD solid solutions. The results presented below, for bulk $WS_2 - WTe_2$, imply that van der Waals interactions may strongly affect phase stabilities, either between adjacent layers in bulk or few-layer samples, or between monolayers and substrates.

Previous work on bulk $(1-X)\cdot MoS_2 - (X)\cdot MoTe_2$ [14] predicted two entropy stabilized incommensurate phases at $X \approx 0.46$, and this work was done to see if a similar prediction applies to the structurally analogous $(1-X)\cdot WS_2 - (X)\cdot WTe_2$ system. In the $WS_2 - WTe_2$ system, however, only a miscibility gap is predicted, but a very large number of formation energy calculations, $N_{str} \lesssim 400$, is required to suppress false ground-states (GS). Also, the asymmetry of the calculated phase diagram is the opposite of what one expects from a size-effect argument [15,16]; typically there is more solubility of the smaller ion in larger-ion-rich solutions (more S-solubility in Te-rich solutions) than vice versa; $R_S = 1.84$ Å; $R_{Te} = 2.21$ Å). [17] In $WS_2 - WTe_2$, phase diagram asymmetry reflects the energy landscape for low-energy metastable states. Miscibility gaps in band-structure engineering materials, such as TMD alloys, are of particular concern to experimentalists because they imply the difficulty (impossibility) of synthesizing homogeneous alloys with continuously varying band-gaps.

2. Methodology

2.1. Total energy calculations

Total structural energies were calculated for fully relaxed WS_2, WTe_2 and for 433 $W_{m+n}(S_mTe_n)_2$ supercells. The Vienna ab initio simulation program (VASP, version 5.3.3 [18,19]) was used for all density-functional theory (DFT) calculations, with projector augmented waves (PAW) and a generalized gradient approximation (GGA) for exchange energies. Electronic degrees of freedom were optimized with a conjugate gradient algorithm. Valence electron configurations were: W_pv $5p^56s5d$; S 3 s^23p^4; Te 5 s^25p^4. Van der Waals interactions were modeled

---

[*] Corresponding author.
E-mail addresses: benjamin.burton@nist.gov (B.P. Burton), m.h.f.sluiter@tudelft.nl (M.H.F. Sluiter).

https://doi.org/10.1016/j.calphad.2018.08.001
Received 12 November 2017; Received in revised form 31 July 2018; Accepted 1 August 2018
0364-5916/ Published by Elsevier Ltd.

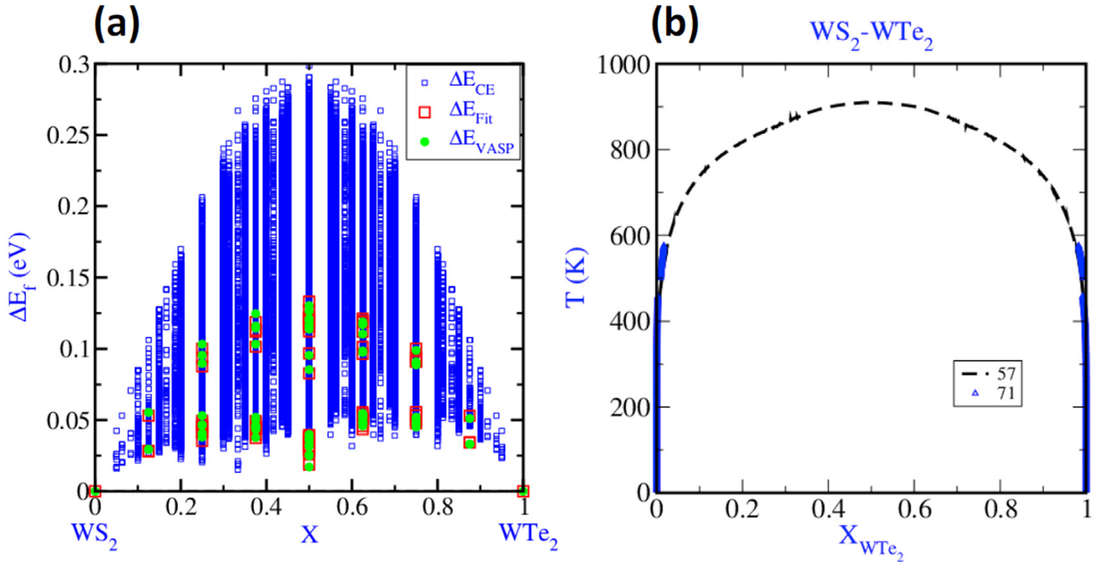

Fig. 1. For $N_{str} = 71$ with $CV = 2.65$ meV/chalcogen atom and $n_{ECI} = 68$, including the point-cluster, 55 pair-, 6 3-body- and 6 4-body interactions: (a) Ground-State analysis; (b) calculated phase diagram. In (a): ΔE_{VASP} filled circles (green online); ΔE_{Fit} large open squares, (red online) is the CEH-fit to the DFT set; ΔE_{CE} smaller open squares, (blue online) are the CEH-based ground-state analysis; All $\Delta E_f > 0$ implies that there are no ordered GS, with 16 or fewer anion sites, and suggests that the phase diagram will have a miscibility gap. Note the small cross-validation score which suggests a very good CEH-fit, and in (b) the near absence of asymmetry in the miscibility gap. (For interpretation of the references to color in this figure legend, the reader is referred to the web version of this article.).

with the non-local correlation functional of Klimes et al. [20]. A 500 eV cutoff-energy was used in the "high precision" option, which converges *absolute* energies to within a few meV/chalogen atom (a few tenths of a kJ/mol of exchangeable S- and Te-anions). Precision is at least an order of magnitude better. Residual forces of order 0.02 eV or less were typical. VASP files describing the 433 total energy calculations are posted in the First Principles Phase Stability Repository. [21]

2.2. The cluster expansion hamiltonian

Cluster expansion Hamiltonians (CEH) [22], were fit to sets of 71, 253, 295, 399, and 435 total energies (zero pressure formation enthalpies),

$$\Delta E_f = \frac{E\left[W_{m+n}(S_m Te_n)_2\right] - mE\left[WS_2\right] - nE\left[WTe_2\right]}{2(m+n)}, \quad (1)$$

where: $E\left[W_{m+n}(S_m Te_n)_2\right]$ is the energy of the $W_{m+n}(S_mTe_n)_2$ supercell. ΔE_f as computed from the ab initio energies, is displayed as solid dots (green online) in Figs. 1a–5a. Fittings of the CEHs were performed with the Alloy Theoretic Automated Toolkit (ATAT) [19,23–25] which automates most CEH construction tasks [24]. In particular the specific effective cluster interactions, *ECI* s, that make up the CEH, and their number n_{ECI}, are chosen by cross validation analysis which selects for the *mostpredictive* CEH; i.e. the CEH that most accurately predicts ΔE_f s that are left out of the fit [26]. The CEH is constructed using a set of pair interactions, 3-body and 4-body interactions. Including many-body interactions is necessary to account for asymmetry in the phase diagram around equi-atomic composition. The inclusion of 4-body terms makes it possible to describe the enthalpy of mixing as a fourth-order polynomial of the composition. Experimental measurements of the enthalpy of mixing, such as through calorimetry, show that generally a fourth order polynomial is sufficient to adequately represent the experimental data [27,28]. As many-body interactions are considered to act as corrections to the contributions from smaller clusters, generally many-body interactions rapidly decay as the number of sites increases. Therefore, the CEH is limited to 4-body ECIs. Note that the number of ab initio structural energies is much larger than n_{ECI}. Therefore, the system of equations for fitting the ECIs is highly overdetermined. Here, the overdeterminedness factor is defined as:

$$\chi = \frac{N_{str}}{n_{ECI}}. \quad (2)$$

$\chi < 1$ indicates a system that has no unique solution; and $\chi = 1$ indicates a system that has a unique solution, provided it is not singular. $\chi > 1$ implies an overdetermined systems in which unique solutions can be defined if an additional criterion is applied such as minimal sum of differences squared.

3. Results

3.1. Ground-state analyses

Filled circles (green online) in Figs. 1a–5a indicate values of ΔE_f that were calculated with the VASP package, i.e. ΔE_{VASP}. Large open squares in Figs. 1a–5a (red online) indicate the CEH-fit to ΔE_{VASP}. Smaller open squares (ΔE_{GS}; blue online) indicate the results of a ground-state (GS) analyses that included all ordered configurations with 16 or fewer anion sites, 151,023 structures. Calculated values for leave-one-out cross validation scores, (CV), and the numbers of structures, N_{str}, are indicated in the figure captions.

Additional GS analyses were performed by Monte-Carlo (MC) simulations at fixed bulk compositions, via decreasing temperature (T) scans down to T = 0. The 0 K ΔE_f values from these calculations are plotted as solid- (predicted stable) or open-diamonds (metastable; blue online) in Fig. 2a and Fig. 3a; and as small filled down-pointing triangles (blue online) in Figs. 4a and 5a. Because the calculated formation energies for the ordered configurations in Figs. 2a and 3a are negative, they constitute (falsely) predicted large-cell ordered-GS. If their formation energies are positive they can be regarded as low-energy microstructures. Note that these formation energies from MC-simulations are always upper bounds, because MC-simulations don't yield *perfectly* ordered simulation boxes.

3.2. Phase diagram calculations

First principles phase diagram calculations that were performed with the ATAT package [23–25] are plotted in Figs. 1b–5b. Additional symbols on Figs. 2b, 3b, and 4b are used to indicate various phase fields